Chiral analysis of quenched baryon masses

R. D. Young,[1] D. B. Leinweber,[1] A. W. Thomas,[1] and S. V. Wright[1,2]
[1]*Special Research Centre for the Subatomic Structure of Matter and Department of Physics and Mathematical Physics, University of Adelaide, Adelaide SA 5005, Australia*
[2]*Division of Theoretical Physics, Department of Mathematical Sciences, University of Liverpool, Liverpool L69 3BX, United Kingdom*
(Received 17 May 2002; published 27 November 2002)

We extend to quenched QCD an earlier investigation of the chiral structure of the masses of the nucleon and the delta in lattice simulations of full QCD. Even after including the meson-loop self-energies which give rise to the leading and next-to-leading nonanalytic behavior (and hence the most rapid variation in the region of light quark mass), we find surprisingly little curvature in the quenched case. Replacing these meson-loop self-energies by the corresponding terms in full QCD yields a remarkable level of agreement with the results of the full QCD simulations. This comparison leads to a very good understanding of the origins of the mass splitting between these baryons.

DOI: 10.1103/PhysRevD.66.094507 PACS number(s): 12.38.Gc, 12.38.Aw, 12.39.Fe, 12.40.Yx

I. INTRODUCTION

The quenched approximation is a widely used tool for studying nonperturbative QCD within numerical simulations of lattice gauge theory. With an appropriate choice of the lattice scale and at moderate to heavy quark masses, this approximation has been shown to give only small, systematic deviations from the results of full QCD with dynamical fermions. Although no formal connection has been established between full and quenched QCD, the similarity of the results has led to the belief that the effects of quenching are small and hence that quenched QCD provides a reasonable approximation to the full theory [1].

Improved lattice actions, together with advances in high performance computing, have been responsible for significant improvements in the calculation of baryon masses at moderate to light quark masses within the quenched approximation [2–5]. Simulations with dynamical fermions have proven to be more difficult, but results have been reported with pion masses as low as 320 MeV [4,6].

The fact that one is restricted to quark masses much larger than the physical values means that, in addition to all the usual extrapolations (e.g., to the infinite volume and continuum limits), if one wants to compare with empirical hadron observables, one must also have a reliable method of extrapolation to the chiral limit. Any such extrapolation must incorporate the appropriate chiral corrections, arising from Goldstone boson loops, which give rise to rapid, nonlinear variations as the chiral limit is approached.

Studies of the exactly soluble Euler-Heisenberg problem [7], suggest that one can develop surprisingly accurate extrapolation functions, provided one builds in the correct behavior in *both* the small and large mass limits. For QCD, Leinweber *et al.* [8] have suggested an extrapolation method which ensures both the exact low mass limit of chiral perturbation theory [technically its leading (LNA) and next-to-leading nonanalytic (NLNA) behavior] and the heavy quark limit of heavy quark effective theory (HQET). The transition between the chiral and heavy quark regimes is characterized by a mass scale Λ, related to the inverse of the size of the pion cloud source.

This approach is equivalent to the formulation of chiral perturbation theory (χPT) using a finite-range regulator with extent governed by Λ [9]. The resummation of the chiral expansion arising from the finite-range regulator suppresses the rapid nonanalytic variation of hadron properties once the pion Compton wavelength is smaller than this scale (i.e. $m_\pi > \Lambda$). The importance of incorporating such behavior has been successfully demonstrated for a number of hadronic observables, including masses [8,10], the sigma commutator [11], magnetic moments [12–15], charge radii [16] and parton distribution functions [17–19].

The impressive results found using these methods have led us to the present investigation of the problem of the chiral extrapolation of baryon masses in quenched QCD. The chiral properties within the quenched approximation are known to differ from those of full QCD in a number of very interesting ways [20–25]. For example, not only are the effective couplings at the pion-baryon vertices significantly altered in quenched QCD (QQCD) but, because the η' behaves as a Goldstone boson in QQCD, one must also consider η' loops.

Here we first review previous work [8] which reported a successful method for extrapolating baryon masses as calculated in full QCD lattice simulations. The modified chiral structure of quenched baryon masses [23] is presented next. We show how to construct the various meson loop induced self-energies [26] in order to preserve the leading-nonanalytic and next-to-leading nonanalytic structure appropriate to QQCD, while incorporating the established behavior at heavier quark masses. This is followed by a detailed application to the extrapolation of the quenched N and Δ masses to the chiral limit. Finally, we use the observed similarity of the structure of baryons stripped of their Goldstone boson clouds, in full and quenched QCD, to explore whether one can make a connection between the masses calculated in QQCD and those obtained in a dynamical simulation. The remarkable agreement obtained suggests a number of further tests and also leads us, with considerable confidence, to an interpretation of the origin of the N-Δ mass splitting.

II. QCD EXTRAPOLATION

In general, the coefficients of the LNA and NLNA terms in a chiral expansion of baryon masses are very large. For instance, the LNA term for the nucleon mass is $\delta m_N^{(\mathrm{LNA})} = -5.6\, m_\pi^3$ (with m_π and $\delta m_N^{(\mathrm{LNA})}$ in GeV). With $m_\pi = 0.5$ GeV, quite a low mass for current simulations, this yields $\delta m_N^{(\mathrm{LNA})} = 0.7$ GeV—a huge contribution. Furthermore, in this region hadron masses in both full and quenched lattice QCD are found to be essentially linear in m_π^2 or equivalently quark mass, whereas $\delta m_N^{(\mathrm{LNA})}$ is highly nonlinear. The challenge is therefore to ensure the appropriate LNA and NLNA behavior, *with the correct coefficients*, as $m_\pi \to 0$, while making the transition to linear behavior as m_π increases, sufficiently rapidly to describe the actual lattice data.

A reliable method for achieving all this was proposed by Leinweber *et al.* [8]. They fit the full (unquenched) lattice data with the form

$$M_B = \alpha_B + \beta_B m_\pi^2 + \Sigma_B(m_\pi, \Lambda), \tag{1}$$

where Σ_B is the total contribution from those pion loops which give rise to the LNA and NLNA terms in the self-energy of the baryon. For the N these correspond to the processes $N \to N\pi \to N$ and $N \to \Delta\pi \to N$, while for the Δ we need $\Delta \to \Delta\pi \to \Delta$ and $\Delta \to N\pi \to \Delta$. Explicitly,

$$\Sigma_N = \sigma_{NN}^\pi + \sigma_{N\Delta}^\pi,$$

$$\Sigma_\Delta = \sigma_{\Delta\Delta}^\pi + \sigma_{\Delta N}^\pi. \tag{2}$$

In the heavy baryon limit, these four contributions ($B \to B'\pi \to B$) can be summarized as

$$\sigma_{BB'}^\pi = -\frac{3}{16\pi^2 f_\pi^2} G_{BB'} \int_0^\infty dk \frac{k^4 u^2(k)}{\omega(k)[\omega_{BB'} + \omega(k)]}, \tag{3}$$

where $\omega(k) = \sqrt{k^2 + m_\pi^2}$ is the intermediate pion energy and $\omega_{BB'} = (M_{B'} - M_B)$ is the physical baryon mass splitting and $f_\pi = 93$ MeV. The coefficients $G_{BB'}$ are standard SU(6) couplings and are summarized in Sec. IV. The ultraviolet regulator, $u(k)$, has a very natural physical interpretation as the Fourier transform of the source of the pion field. The LNA and NLNA structure of these diagrams is associated with the infrared behavior of the corresponding integrals and hence is independent of the choice of regularization scheme. The use of such a regulator effectively suppresses the self-energies like Λ^2/m_π^2 for $m_\pi \gg \Lambda$, the characteristic mass scale of the cutoff. A common choice of regulator, which we use throughout this work, is the dipole form, $u(k) = \Lambda^4/(\Lambda^2 + k^2)^2$.

In terms of the underlying effective field theory, the shape of the regulator is irrelevant to the formulation of χPT [9]. However, current lattice simulation results encourage us to look for an efficient formulation which maximizes the applicable pion-mass range accessed via one- or two-loop order. An optimal regulator (motivated by phenomenology) will effectively re-sum the chiral expansion encapsulating the physics in the first few terms of the expansion. The approach is systematically improved by simply going to higher order in the chiral expansion. Our experience with dipole and monopole vertex regulators indicates that the shape of the regulator has little effect on the extrapolated results, provided lattice QCD simulation results are used to constrain the optimal regulator parameter on an observable-by-observable basis [8,10].

In a phenomenological sense, the linear term of Eq. (1), which dominates for $m_\pi \gg \Lambda$, encompasses the quark mass dependence of the pion-cloud source—the baryon without its pion dressing. This term also serves to account for loop diagrams involving heavier mesons (integrated out of the effective field theory), which have much slower variation with quark mass. Given the current state of the art in lattice simulations, data in the low to intermediate mass range are unable to reliably constrain the optimal parameter Λ. There is considerable phenomenological support for choosing a dipole regulator parameter somewhat smaller than found for the axial form factor of the nucleon, which is 1.03 ± 0.04 GeV [27–29]. However, it is important to understand that the anticipated development of supercomputing resources and techniques are such that Λ may be optimally constrained by full QCD simulation data in the near future.

Fitting lattice results to Eq. (1) is straightforward. Upon calculating the described self-energies for a given choice of Λ, the fitting procedure amounts to a simple linear fit in α_B and β_B.

III. QUENCHED CHIRAL PERTURBATION THEORY

Standard chiral perturbation theory is a low energy effective field theory built upon the symmetries of QCD [30,31]. It amounts to an expansion of Green's functions in powers of momenta and quark mass about the chiral limit ($m_q = 0$). In the case of baryon masses, χPT tells us the leading behavior of the quark mass expansion. Because χPT is an effective field theory, the renormalization procedure must be performed order by order in perturbation theory. At higher and higher order, more and more unknown parameters are introduced. These unknowns only play a role in analytic terms of the expansion. The coefficients of the leading nonanalytic terms are constrained by chiral symmetry [32]—they are independent of regularization and the order of the chiral expansion. In connecting the results of lattice QCD to the physical world it is essential that one incorporate the correct nonanalytic structure of the low energy theory.

Quenched χPT (QχPT) provides the analogous low energy effective theory for QQCD [21–23]. Sea quark loops are removed from QCD by including a set of degenerate, commuting (bosonic) quark fields. These bosonic fields have the effect of exactly cancelling the fermion determinant in the functional integration over the quark fields. This gives a Lagrangian for a field theory which is equivalent to the quenched approximation simulated on the lattice. The low energy effective theory is then constructed on the basis of the symmetries of this Lagrangian.

The leading chiral expansion of baryon masses in the quenched approximation has been calculated by Labrenz and

TABLE I. Coefficients of the lowest order nonanalytic terms in the chiral expansions of the N and Δ masses, with values from both full and quenched QCD listed for comparison ($\nu^{-1}=16\pi f_\pi^2$, $\Delta M = M_\Delta - M_N$).

B	c_i	QCD	QQCD
N	c_1	0	$-\frac{1}{2}(3F-D)^2 m_0^2 \nu$
	c_3	$-\frac{3}{2}(F+D)^2 \nu$	$\{\frac{4}{3}(D^2-3DF)-2(3F-D)\gamma\}\nu$
	c_{4L}	$\frac{3}{\pi}(F+D)^2 \frac{32}{25}\frac{3}{8\Delta M}\nu$	$\frac{\mathcal{C}^2}{2\pi\Delta M}\nu$
Δ	c_1	0	$-\frac{5}{18}\mathcal{H}^2 m_0^2 \nu$
	c_3	$-\frac{3}{2}(F+D)^2 \nu$	$\{-\frac{10}{27}\mathcal{H}^2-\frac{10}{9}\mathcal{H}\gamma'\}\nu$
	c_{4L}	$-\frac{3}{\pi}(F+D)^2 \frac{8}{25}\frac{3}{8\Delta M}\nu$	$\frac{\mathcal{C}^2}{2\pi\Delta M}\frac{4}{25}\nu$

Sharpe [23]. For the reasons already mentioned in the Introduction, it differs from the corresponding expansion in full QCD. In particular, the chiral expansion coefficients take different values and new, nonanalytic behavior is also introduced. The explicit form can be expressed as

$$M_B = M_B^{(0)} + c_1^B m_\pi + c_2^B m_\pi^2 + c_3^B m_\pi^3 + c_4^B m_\pi^4 + c_{4L}^B m_\pi^4 \log m_\pi + \ldots \quad (4)$$

with the coefficients of the terms which are nonanalytic in the quark mass listed in Table I. We note that in Ref. [23] the N and Δ were treated as degenerate states in the chiral limit. Experience in other situations suggests that it is more accurate to retain a finite mass difference, in which case off–diagonal terms such as $N\to\Delta\pi\to N$ lead to the nonanalytic behavior of the form $m_\pi^4 \log m_\pi$.

The contribution linear in m_π is unique to the quenched approximation. The quenched theory therefore exhibits a more singular behavior in the chiral limit. The origin of this behavior is the Goldstone nature of the η' in QQCD and specifically the process shown in Fig. 1(b). We note also that the coefficients of the chiral expansion involve new couplings, γ and γ', which are related to the flavor-singlet, hairpin-baryon couplings for N and Δ respectively, illustrated in Fig. 1(a). In the formalism of Ref. [23] these are related to the couplings of full QCD via the relations

$$\gamma = D - F, \qquad \gamma' = 0, \quad (5)$$

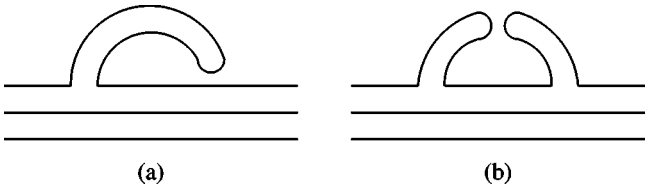

FIG. 1. Quark flow diagrams for the chiral η' loop contributions appearing in QQCD: (a) single hairpin, (b) double hairpin.

TABLE II. Chiral couplings appearing in the self-energy integrals, Eq. (3) for full QCD and Eq. (6) for QQCD. In numerical calculations we have used the couplings arising from $SU(6)$ relations [34], $\mathcal{C}=-2D$ and $\mathcal{H}=-3D$.

	G_{NN}	$G_{N\Delta}$	$G_{\Delta\Delta}$	$G_{\Delta N}$
QCD	$(F+D)^2$	$\frac{32}{25}(F+D)^2$	$(F+D)^2$	$\frac{8}{25}(F+D)^2$
QQCD	$\frac{8}{9}(3DF-D^2)$	$\frac{16}{9}D^2$	$\frac{20}{9}D^2$	$-\frac{8}{9}D^2$

as described in Appendix B. There is some uncertainty over the flavor singlet couplings, especially in connection with Okubo-Zweig-Iizuka (OZI) violation associated with the U(1) axial anomaly [33]. While this may modify our calculated curves at extremely light quark mass, it would have no significant effect on the fit to lattice data at large quark mass nor on the comparison of current quenched and full QCD data.

IV. QUENCHED SELF-ENERGIES

Our aim is to apply a similar procedure for the chiral extrapolation of quenched QCD data to that which has proven successful for the physical theory. That is, we wish to generalize Eq. (1) to replace the LNA and NLNA self-energy terms arising in full QCD by their quenched analogues. The pion loop contributions have the same kinematic structure as those in full QCD. A simple redefinition of the couplings, $G_{BB'}$, in the expressions for the self-energies ensures that the correct LNA and NLNA of QχPT is maintained. Thus, the analytic expressions for the pion cloud corrections to the masses of the N and Δ are of the same form as the full QCD integrals [c.f. Eq. (3)]:

$$\tilde{\sigma}_{BB'}^{\pi} = -\frac{3}{16\pi^2 f_\pi^2}\tilde{G}_{BB'}\int_0^\infty dk \frac{k^4 u^2(k)}{\omega(k)[\omega_{BB'}+\omega(k)]}, \quad (6)$$

where the quenched couplings, $\tilde{G}_{BB'}$, are listed in Table II, together with their physical counterparts. Assuming a weak N_f dependence of the chiral parameters, we describe the quenched self-energies using the same tree level values of $D=0.76$ and $F=0.50$ as in full QCD.

Within the quenched approximation η' loops also contribute to the low energy effective theory, whereas they are usually neglected in the physical case. This is because a resummation of internal loop diagrams (coming from the fermion determinant) means that the η' remains massive in the chiral limit of full QCD. On the other hand, the absence of these virtual loops in the quenched approximation causes the flavor singlet η' to behave as a Goldstone boson [21,22]. As a consequence of this feature of the quenched theory, there are two new types of loop contributions to be considered. A schematic view of these processes is shown in Fig. 1.

The first of these two contributions, shown in Fig. 1(a), arises from a single ''hairpin'' interaction. As discussed above, it is responsible for the term proportional to γ (γ') in the chiral expansion of the N (Δ) mass. These couplings are discussed in considerable detail in Appendix B. The structure

TABLE III. Couplings used in flavor singlet η' self-energies. We take $m_0^2 = 0.42$ GeV^2, lying between phenomenological and lattice estimates [35–37]. The momentum dependence of the double hairpin vertex, which is believed to be small, is neglected.

	$N_B^{(1)}$	$N_B^{(2)}$ (GeV^2)
N	$\frac{4}{3}(3F-D)\gamma$	$\frac{2}{9}(3F-D)^2 m_0^2$
Δ	$\frac{20}{27}\mathcal{H}\gamma'$	$\frac{10}{81}\mathcal{H}^2 m_0^2$

of this diagram is exactly the same as the pion loop contribution where the internal baryon is degenerate with the external state. The integral representing this diagram is then the same as that for $\tilde{\sigma}^{\pi}_{BB}$,

$$\tilde{\sigma}_B^{\eta'(1)} = -\frac{3}{16\pi^2 f_\pi^2} N_B^{(1)} \int_0^\infty dk \frac{k^4 u^2(k)}{\omega^2(k)}. \tag{7}$$

The factors $N_B^{(1)}$, providing the correct nonanalytic behavior in the chiral expansion [Eq. (4)], are displayed in Table III.

The second of these new η' loop diagrams arises from the double hairpin vertex, pictured in Fig. 1(b). This contribution is particularly interesting because there are two meson propagators and it is therefore responsible for the nonanalytic term linear in m_π—this term being unique to the quenched case. The integral corresponding to this self energy can be written in a similar way:

$$\tilde{\sigma}_B^{\eta'(2)} = \frac{3}{16\pi^2 f_\pi^2} N_B^{(2)} \int_0^\infty dk \frac{k^4 u^2(k)}{\omega^4(k)}. \tag{8}$$

Note the sign change and the higher power of ω in the denominator. The coefficients, $N_B^{(2)}$, providing the correct nonanalytic behavior in Eq. (4)—in this case the coefficient of m_π—are given in Table III. The sum of these four contributions then gives the net meson-loop induced self-energies within the quenched approximation,

$$\tilde{\Sigma}_B = \tilde{\sigma}^{\pi}_{BB} + \tilde{\sigma}^{\pi}_{BB'} + \tilde{\sigma}_B^{\eta'(1)} + \tilde{\sigma}_B^{\eta'(2)}. \tag{9}$$

The individual contributions to the N and Δ masses over a range of pion mass are plotted in Figs. 2 and 3. These are all evaluated with the dipole regulator mass parameter $\Lambda = 0.8$ GeV. The corresponding self-energies from full QCD are also shown for comparison. We note that in QQCD the contributions are typically quite a bit smaller and the double-hairpin graph, $\tilde{\sigma}_B^{\eta'(2)}$, is repulsive. The differences are enhanced for the Δ where $\tilde{\sigma}^{\pi}_{\Delta N}$ is also repulsive. We observe that the rapid, nonlinear behavior (which is effectively much larger in full QCD) is restricted to the region $m_\pi^2 \lesssim 0.2$ GeV^2, above which the self-energies are quite smoothly varying functions of the quark mass.

V. FITTING PROCEDURE

The lattice data considered in this analysis come from the recent paper of Bernard *et al.* [4]. These simulations were performed using an improved Kogut-Susskind quark action, which is known to have good scaling properties [38]. Unlike the standard Wilson fermion action, masses determined at finite lattice spacing are excellent estimates of the continuum limit results.

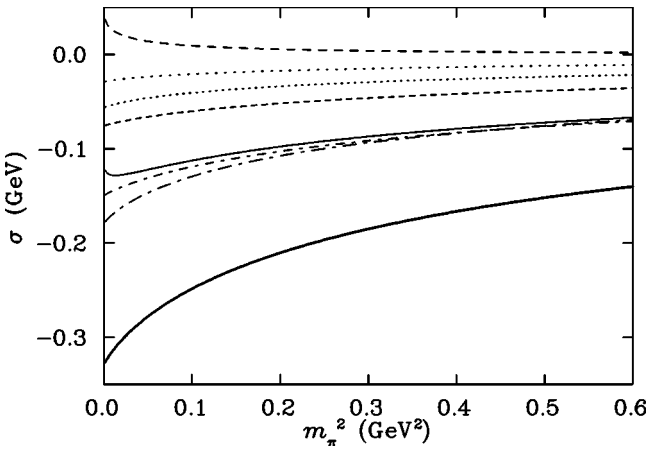

FIG. 2. Various self-energy contributions to M_N for dipole mass, $\Lambda = 0.8$ GeV. From top down at $m_\pi^2 = 0.1$ GeV^2, the curves correspond to (where a $\sim$ over the symbol denotes a quenched QCD contribution) $\tilde{\sigma}_N^{\eta'(2)}, \tilde{\sigma}_N^{\eta'(1)}, \tilde{\sigma}^{\pi}_{NN}, \tilde{\sigma}^{\pi}_{N\Delta}$, total quenched $\tilde{\Sigma}_N$, $\sigma^{\pi}_{N\Delta}$, σ^{π}_{NN} and total physical Σ_N.

We are particularly concerned with the chiral extrapolation of baryon masses and how their behavior is affected by the quenched approximation. In such a study, it is essential that the method of scale determination be free from chiral contamination. One such method involves the static-quark potential. As low-lying pseudoscalar mesons made of light quarks exhibit negligible coupling to hadrons containing only heavy valence quarks, the low energy effective field theory plays no role in the determination of the scale for these systems. In fixing the scale through such a procedure one constrains all simulations, quenched, 2-flavor, 3-flavor

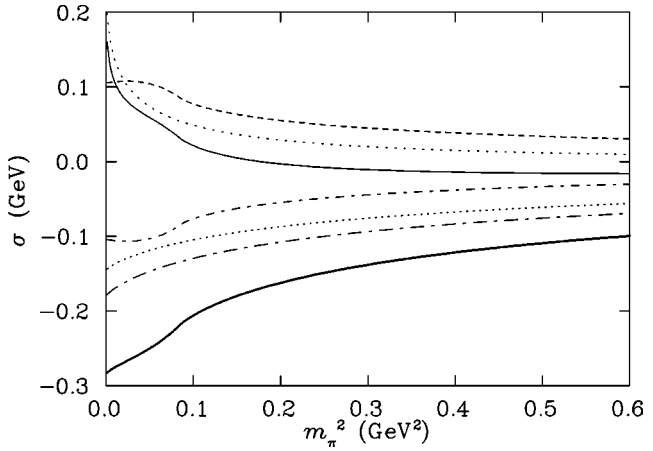

FIG. 3. Various self-energy contributions to M_Δ for dipole mass, $\Lambda = 0.8$ GeV. From top down at $m_\pi^2 = 0.1$ GeV^2, the curves correspond to (where a $\sim$ over the symbol denotes a quenched QCD contribution) $\tilde{\sigma}^{\pi}_{\Delta N}, \tilde{\sigma}_\Delta^{\eta'(2)}$, total quenched $\tilde{\Sigma}_\Delta$, $\sigma^{\pi}_{\Delta N}$, $\tilde{\sigma}^{\pi}_{\Delta\Delta}$, $\sigma^{\pi}_{\Delta\Delta}$ and total physical Σ_Δ.

etc., to match phenomenological static-quark forces. Effectively, the short range (0.35–0.5 fm) interactions are matched across all simulations.

A commonly adopted method involving the static-quark potential is the Sommer scale [39,40]. This procedure defines the force, $F(r)$, between heavy quarks at a particular length scale, namely $r_0 \simeq 0.5$ fm. Choosing a narrow window to study the potential avoids complications arising in dynamical simulations where screening and ultimately string breaking is encountered at large separations. The lattice data analyzed in this report use a variant of this definition, choosing to define the force at $r_1 = 0.35$ fm via $r_1^2 F(r_1) = 1.00$ [4].

As we remarked earlier, the nonanalytic chiral behavior is governed by the infrared regions of the self-energy integrals. The fact that the lattice calculations are performed on a finite volume grid means that the self-energy integrals implicit in current lattice simulations do not include the exact chiral behavior. It is important to take this into account in the fitting procedure and we therefore follow Ref. [10] in replacing the continuum self-energy integrals used in the fitting process by a discrete sum over the meson momenta available on the lattice:

$$4\pi \int_0^\infty k^2 dk = \int d^3k \approx \frac{1}{V}\left(\frac{2\pi}{a}\right)^3 \sum_{k_x,k_y,k_z}. \qquad (10)$$

The self-energy integrals calculated in this way are what should be directly compared with the lattice data, and we illustrate these by open squares in subsequent figures. Upon obtaining the optimal fit parameters, one can evaluate the integrals exactly and therefore obtain the infinite-volume, continuum limit. The latter is the result which should be compared with experiment at the physical pion mass.

We now proceed to fit quenched lattice data with the form

$$\tilde{M}_B = \tilde{\alpha}_B + \tilde{\beta}_B m_\pi^2 + \tilde{\Sigma}_B(m_\pi, \Lambda) \qquad (11)$$

[by analogy with the form used in full QCD, Eq. (1)], with the self-energies evaluated, as we have just outlined, using the momentum grid corresponding to the specific lattice simulation. Phenomenologically speaking, the linear terms in Eq. (11) may be thought of as accounting for the quark mass dependence of the pion-cloud source. This form then automatically includes the expected heavy quark behavior where the π and η' loop contributions are suppressed.

The effective field theory regulator, motivated by the physical structure of the meson-baryon vertex, characterizes the finite size of the pion source. Quenched simulations of hadronic charge radii performed at moderate to heavy quark masses [41] have been demonstrated to be consistent with experiment once the meson-cloud properties of full QCD are taken into account [16,42]. This indicates that the size of the meson-cloud source is expected to be of similar size in both quenched and physical QCD. For this reason we proceed to fit both quenched and physical data with a common value of Λ. For a fixed choice of Λ, fitting to lattice data amounts to a linear fit in α and β. It turns out that, for a range of values of Λ, the values of α and β found for the QQCD data are surprisingly close to the values found for the fit to dynamical QCD data. This strongly suggests that the self-energies included here, which contain the LNA and NLNA behavior appropriate to each type of simulation, contain the primary effect of quenching. To illustrate the point, Fig. 4 shows a measure, δ, of the difference between the quenched and dynamical data sets over the range of m_π considered. This measure is proportional to the net area contained between the straight lines obtained from the fits and has been normalized to the case where the self-energy diagrams are totally neglected. The improved agreement between data sets over the range of dipole masses highlights the effectiveness of this self-energy correction. It is also worth noting that the χ^2/d.o.f. is also improved by incorporating the self-energies into the fit. For the preferred dipole mass, $\Lambda = 0.8$ GeV, this is better by a factor 2. Results of both the physical and quenched fits are shown together in Fig. 5. The parameters of the best fits are displayed in Table IV. Here we see the remarkable agreement of the linear term of our fitting formulas, Eqs. (1) and (11). This strongly suggests that the behavior of the meson-cloud source is very similar in quenched and full QCD. The primary difference between the quenched and physical results can then be described by the meson-loop induced self-energies.

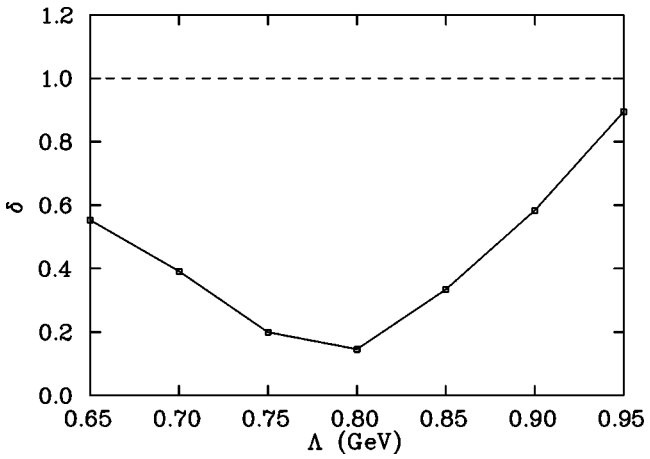

FIG. 4. The value δ is a measure of the difference between the quenched and dynamical data sets after accounting for the relevant self-energy diagrams. This measure is proportional to the net area contained between the straight lines obtained from the fits and has been normalized to the case where the self-energy diagrams are totally neglected.

This observation suggests that it may well be possible to make a connection between quenched simulations and hadron properties in the real world. One would fit quenched data with appropriate self-energies to obtain the linear behavior of the meson-cloud source. Then the quenched self-energies would be replaced by their full-QCD counterparts, hence obtaining more physical results. It is clearly very important to test this result further on other hadrons (e.g. for other members of the octet) and against dynamical simulations at lower quark masses.

VI. Δ-N HYPERFINE SPLITTING

The analysis of lattice data has demonstrated the ability to describe the primary difference between quenched and dy-

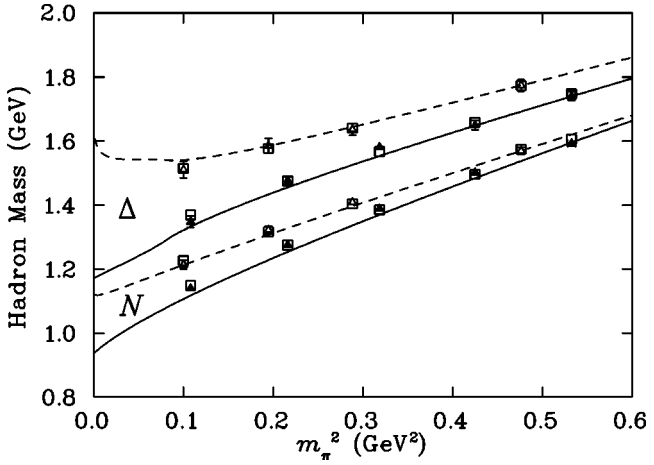

FIG. 5. Fit (open squares) to lattice data [4] (quenched △, dynamical ▲) with adjusted self-energy expressions accounting for finite volume and lattice spacing artifacts. The infinite-volume, continuum limit of quenched (dashed lines) and dynamical (solid lines) are shown. The lower curves and data points are for the nucleon and the upper ones for the Δ.

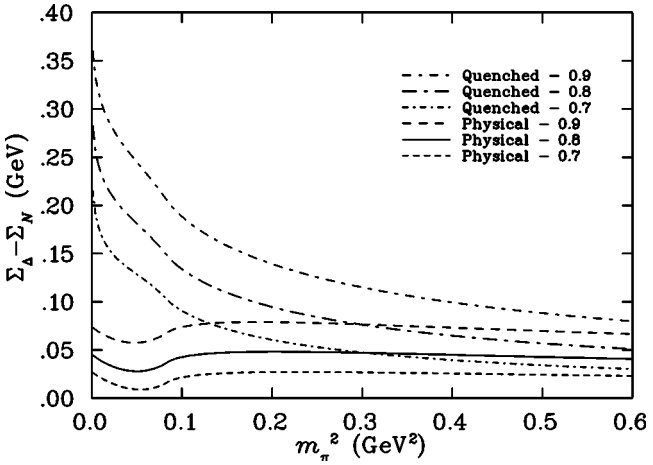

FIG. 6. Meson-loop contribution to the Δ-*N* mass splitting in both quenched and full QCD—for several values of the dipole mass.

namical simulations in terms of the meson-loop self-energies. Figure 6 shows the difference in the self-energy terms for the *N* and Δ in quenched and full QCD, for several values of the common dipole-regulator mass. It is quite clear that there is a difference of between 150 and 250 MeV between the quenched and full QCD cases. Since this difference was essential in accounting for the clear differences in the behavior of the baryon masses in QQCD and full QCD shown in Fig. 5, we have some confidence in using these results to say how much of the physical *N*-Δ mass splitting is associated with pion loops and how much comes from short range processes, such as gluon exchange. In fact, an examination of Fig. 6 for the case of full QCD suggests fairly clearly that only about 50 MeV of the observed 300 MeV *N*-Δ splitting arises from pion loops. Of course, this result is more dependent on the assumption of the *same* dipole mass parameter at every vertex than the fits to the *N* and Δ masses individually. Nevertheless, it seems unlikely that more than a third of the total splitting could come from this source.

VII. CONCLUSIONS

We have investigated the quark mass dependence of the *N* and Δ masses within the quenched approximation. The leading chiral behavior of hadron masses is known to differ in quenched QCD from the physical theory. This knowledge has been used to guide us in the construction of an effective field theory which encompasses the correct chiral structure, and is consistent with current lattice simulations. This procedure of fitting lattice data with a linear term together with the meson-loop corrections which give rise to the LNA and NLNA behavior has been demonstrated previously to fit dynamical QCD simulation results remarkably well. Here we have shown that the application of the same procedure to quenched results is able to consistently fit the data in that case as well. We note that this approach encapsulated in Eqs. (1) and (11) is a finite-range regulated effective field theory consistent with the traditional dimensional regularization approach to χPT. By calculating next-order loop contributions it is systematically improvable and model independent [9].

Remarkably, a comparison of the two fits suggests that the properties of the *N* and Δ, stripped of their pion clouds, are essentially the same in quenched and full QCD, once the scale is set using the Sommer scale appropriate to heavy quark systems. This observation is dependent on an optimal regulator shape and size, and the assumption that the axial coefficients are similar in quenched and full QCD. Therefore this result should be regarded as a phenomenological link. The extent to which this observation is model independent requires the investigation of alternative regulators and new accurate lattice results approaching the light quark-mass regime. At present, the success of this result further motivates use of the phenomenologically preferred dipole, which gives a most accurate description of the shape of the pion-cloud source. It is clearly essential to test this finding against further full QCD simulations at lighter quark masses as well as for other hadrons.

We have demonstrated that although the quenched approximation gives rise to more singular behavior in the chiral limit, this is not likely to be observed in lattice simulations as these contributions are quickly suppressed with increasing quark mass. Indeed our results suggest that it will be very

TABLE IV. Best fit parameters for both full and quenched data sets with dipole regulator, $\Lambda = 0.8$ GeV. The second set correspond to a simple linear fit, where the self-energy contributions have been neglected. All masses are in GeV.

Self-energy	Simulation	α_N	β_N	α_Δ	β_Δ
Dipole	Physical	1.27(2)	0.90(5)	1.45(3)	0.74(8)
	Quenched	1.24(2)	0.85(6)	1.45(4)	0.72(11)
Nil	Physical	1.04(2)	1.07(5)	1.28(3)	0.88(8)
	Quenched	1.14(2)	0.92(6)	1.44(4)	0.69(11)

hard to detect any significant chiral curvature in the case of the nucleon, while for the Δ there may be some small, upward curvature. The Δ-N mass splitting increases to around 400 MeV at the physical point in QQCD. As a consequence of this behavior, the Δ mass in the quenched approximation is expected to differ from the physical mass by approximately 25%. Finally, we have shown that while a fraction of the physical N-Δ mass difference can be attributed to a difference in pion self-energy loops, this is unlikely to amount to more than a third of the observed splitting.

ACKNOWLEDGMENTS

We would like to thank S. Sharpe for numerous enlightening discussions concerning QχPT as well as W. Detmold, M. Oettel, A. Williams and J. Zanotti for helpful conversations. This work was supported by the Australian Research Council and the University of Adelaide.

APPENDIX A: ANALYTIC INTEGRATION

Here we summarize analytic expressions for the self-energy integrals. It should be noted that these expressions are not used in fitting lattice data. For the purpose of fitting, the continuum integral is replaced by a discrete sum over the available momenta on the corresponding lattice, as described in Eq. (10).

Firstly we consider the case of the simple meson-loop digram where the internal baryon line has degenerate mass with the external state:

$$\sigma = -\frac{3}{16\pi^2 f_\pi^2} G \int_0^\infty dk \frac{k^4 u^2(k)}{\omega^2(k)}. \tag{A1}$$

Using a sharp cutoff, $u(k)=\theta(\Lambda-k)$, the integral can be expressed as

$$\sigma = -\frac{3G}{16\pi^2 f_\pi^2}\left[m_\pi^3 \arctan\left(\frac{\Lambda}{m_\pi}\right) + \frac{\Lambda^3}{3} - \Lambda m_\pi^2 \right]. \tag{A2}$$

The LNA behavior of this can then be immediately read from this,

$$\sigma|^{\mathrm{LNA}} = -\frac{3G}{32\pi f_\pi^2} m_\pi^3. \tag{A3}$$

Alternatively, our preferred dipole $u(k)=\Lambda^4/(\Lambda^2+k^2)^2$, also provides an analytic expression for this self-energy,

$$\sigma = -\frac{3G}{512\pi f_\pi^2} \frac{\Lambda^5}{(\Lambda+m_\pi)^4}(m_\pi^2 + 4\Lambda m_\pi + \Lambda^2). \tag{A4}$$

This gives precisely the same LNA behavior as the sharp cutoff, as expected because the nonanalytic behavior is due to the infrared behavior of the integral. It is associated with the residue of the pion propagator pole, and hence independent of an ultraviolet cutoff.

The case of the double meson propagator can also be performed analytically,

$$\sigma = \frac{3}{16\pi^2 f_\pi^2} N \int_0^\infty dk \frac{k^4 u^2(k)}{\omega^4(k)}. \tag{A5}$$

For $u(k)=\theta(\Lambda-k)$,

$$\sigma = \frac{3}{16\pi^2 f_\pi^2} \times N \frac{3m_\pi^2\Lambda + 2\Lambda^3 - 3m_\pi(m_\pi^2+\Lambda^2)\arctan\left(\frac{\Lambda}{m_\pi}\right)}{2(m_\pi^2+\Lambda^2)}. \tag{A6}$$

For $u(k)=\Lambda^4/(\Lambda^2+k^2)^2$,

$$\sigma = \frac{3N}{512\pi f_\pi^2} \frac{\Lambda^5(m_\pi+5\Lambda)}{(\Lambda+m_\pi)^5}. \tag{A7}$$

Once again both integrals give the same LNA behavior,

$$\sigma|^{\mathrm{LNA}} = -\frac{9N}{64\pi f_\pi^2} m_\pi. \tag{A8}$$

For the off-diagonal contributions, where the internal baryon is not degenerate with the external state,

$$\sigma = -\frac{3}{16\pi^2 f_\pi^2} G \int_0^\infty dk \frac{k^4 u^2(k)}{\omega(k)[\omega_{BB'}+\omega(k)]}, \tag{A9}$$

with $\omega_{BB'}$ finite. The results do not have a simple form. The full expression for the case of a sharp cutoff form factor can be found in Ref. [8]. We show the LNA contribution to this diagram for reference,

$$\sigma|^{\mathrm{LNA}} = -\frac{9G}{128\,\pi^2 f_\pi^2} \frac{m_\pi^4}{\omega_{BB'}} \log m_\pi. \tag{A10}$$

APPENDIX B: FLAVOR SINGLET IN FULL AND QUENCHED QCD

This appendix serves to clarify the derivation of the hairpin meson-baryon couplings in quenched χPT.

The flavor singlet η' remains light in the quenched approximation, and is therefore an effective degree of freedom in the low energy sector. Such excitations must therefore be incorporated into the low-energy analysis. Within full QCD, resummation of internal loop diagrams renders the η' massive and hence it plays no role in the low-energy dynamics. For this reason couplings to such flavor singlet states are neglected. In our analysis, we wish to compare the low-energy structure of the quenched and physical theories. In this case, a flavor singlet coupling, like $NN\eta'$, must be included in the chiral Lagrangian of full QCD in order that it is

treated on equal footing with the quenched theory. This coupling will not alter any results of the physical theory as any diagram would involve the propagation of a heavy η'.

Here we derive best estimates for the flavor singlet couplings in quenched QCD. This is achieved by comparison of the quenched and full chiral Lagrangians, under the standard assumption that the couplings exhibit negligible change between the two theories [23]. We follow the notation of Labrenz and Sharpe [23] in the analysis of such contributions. All symbols retain the same meaning, unless otherwise specified.

The chiral Lagrangian for full QCD can be expressed as

$$\mathcal{L}=\mathcal{L}_{\pi}+\mathcal{L}_{B\pi}+\mathcal{L}_{T\pi}. \tag{B1}$$

The standard octet and decuplet Lagrangians are given with an additional coupling to an SU(3) flavor singlet state. For clarity we label the octet and singlet parts of the meson matrix, A:

$$\mathcal{L}_{B\pi}=i\,\mathrm{tr}(\bar{B}v\cdot\mathcal{D}B)+2D\,\mathrm{tr}(\bar{B}S^{\mu}\{A_{\mu}^{oct},B\})+2F\,\mathrm{tr}(\bar{B}S^{\mu}[A_{\mu}^{oct},B])+2\mu b_D\,\mathrm{tr}(\bar{B}\{\mathcal{M}^{+},B\})+2\mu b_F\,\mathrm{tr}(\bar{B}[\mathcal{M}^{+},B])$$
$$+2\mu b_0\,\mathrm{tr}(\bar{B}B)\,\mathrm{tr}(\mathcal{M}^{+})+2g_s\,\mathrm{tr}(\bar{B}S^{\mu}B)\,\mathrm{tr}(A_{\mu}^{sin}), \tag{B2}$$

$$\mathcal{L}_{T\pi}=-i\bar{T}^{\nu}(v\cdot\mathcal{D})T_{\nu}+\Delta M\bar{T}^{\nu}T_{\nu}+2\mathcal{H}\bar{T}^{\nu}S^{\mu}A_{\mu}^{oct}T_{\nu}+\mathcal{C}(\bar{T}^{\nu}A_{\nu}^{oct}B+\bar{B}A_{\nu}^{oct}T^{\nu})+c\bar{T}^{\nu}\mathcal{M}^{+}T_{\nu}-\bar{\sigma}\bar{T}^{\nu}T_{\nu}\,\mathrm{tr}(\mathcal{M}^{+})$$
$$+2g_s'\bar{T}^{\nu}S^{\mu}T_{\nu}\,\mathrm{tr}(A_{\mu}^{sin}). \tag{B3}$$

The new parameters, g_s and g_s', describe couplings of the flavor singlet η' to baryon octet and decuplet states respectively. Within full QCD the single vertex has two topologically different quark flow diagrams as illustrated by the left and right-hand vertices of Fig. 1(a). The left is that of a $q\bar{q}$ insertion on one of the valence quark lines and the right is a pure gluonic coupling through a hairpin-style $q\bar{q}$ annihilation. The total coupling is a sum of these two contributions. Denoting the hairpin vertex coupling by γ_{QCD} and γ'_{QCD} for octet and decuplet baryons respectively we have

$$g_s=\frac{1}{\sqrt{6}}g_{\eta' NN}+\gamma_{\mathrm{QCD}}, \tag{B4}$$

$$g_s'=\frac{1}{\sqrt{6}}g_{\eta'\Delta\Delta}+\gamma'_{\mathrm{QCD}}. \tag{B5}$$

The first of these interactions, $g_{\eta' NN}$ ($g_{\eta'\Delta\Delta}$) is related to the axial couplings by SU(6) phenomenology. We take the standard approach and assign

$$g_{\eta' NN}=\sqrt{2}g_{\eta NN}=\sqrt{\frac{2}{3}}(3F-D), \tag{B6}$$

$$g_{\eta'\Delta\Delta}=\sqrt{2}g_{\eta\Delta\Delta}=\sqrt{\frac{2}{3}}\mathcal{H}. \tag{B7}$$

The effective chiral Lagrangian of quenched QCD is [23]

$$\mathcal{L}^{(Q)}=\mathcal{L}_{\Phi}^{(Q)}+\mathcal{L}_{\mathcal{B}\Phi}^{(Q)}+\mathcal{L}_{\mathcal{T}\Phi}^{(Q)}, \tag{B8}$$

where meson and baryon states are now understood to be constructed of ordinary quarks and bosonic quarks. The general Lagrangian for the heavy fields can be written in terms of the rank-3 tensor fields as defined in Ref. [23], $\mathcal{B}$ and $\mathcal{T}$,

$$\mathcal{L}_{\mathcal{B}\Phi}^{(Q)}=i(\bar{\mathcal{B}}v\cdot\mathcal{D}\mathcal{B})+2\alpha(\bar{\mathcal{B}}S^{\mu}\mathcal{B}A_{\mu})+2\beta(\bar{\mathcal{B}}S^{\mu}A_{\mu}\mathcal{B})$$
$$+2\gamma_s(\bar{\mathcal{B}}S^{\mu}\mathcal{B})\,\mathrm{str}(A_{\mu})+\alpha_M(\bar{\mathcal{B}}\mathcal{B}\mathcal{M}^{+})+\beta_M(\bar{\mathcal{B}}\mathcal{M}^{+}\mathcal{B})$$
$$+\sigma(\bar{\mathcal{B}}\mathcal{B})\,\mathrm{str}(\mathcal{M}^{+}), \tag{B9}$$

$$\mathcal{L}_{\mathcal{T}\Phi}^{(Q)}=-i(\bar{\mathcal{T}}^{\nu}(v\cdot\mathcal{D})\mathcal{T}_{\nu})+\Delta M(\bar{\mathcal{T}}^{\nu}\mathcal{T}_{\nu})+2\mathcal{H}(\bar{\mathcal{T}}^{\nu}S^{\mu}A_{\mu}\mathcal{T}_{\nu})$$
$$-\sqrt{\frac{3}{2}}\mathcal{C}[\bar{\mathcal{T}}^{\nu}A_{\nu}\mathcal{B}+\bar{\mathcal{B}}A_{\nu}\mathcal{T}^{\nu}]+2\gamma_s'(\bar{\mathcal{T}}^{\nu}S^{\mu}\mathcal{T}_{\nu})\,\mathrm{str}(A_{\mu})$$
$$+c\bar{\mathcal{T}}^{\nu}\mathcal{M}^{+}\mathcal{T}_{\nu}-\bar{\sigma}(\bar{\mathcal{T}}^{\nu}\mathcal{T}_{\nu})\,\mathrm{tr}(\mathcal{M}^{+}). \tag{B10}$$

It should be noted that the terms γ_s and γ_s' describe both types of flavor-singlet coupling, not just that arising through the hairpin alone. Similarly to Eq. (B5), in the quenched theory these can be described by

$$\gamma_s=\frac{1}{\sqrt{6}}g_{\eta' NN}+\gamma, \tag{B11}$$

$$\gamma_s'=\frac{1}{\sqrt{6}}g_{\eta'\Delta\Delta}+\gamma', \tag{B12}$$

where the terms γ and γ' now correspond to the pure hairpin couplings as used in Ref. [23]. Here we also note the terms $g_{\eta' NN}$ and $g_{\eta'\Delta\Delta}$ are unchanged in going to the quenched theory; this is consistent with the assumption that the chiral parameters F and D are unchanged between the two theories.

One can then relate the quenched chiral Lagrangian back to that of full QCD by restricting the indices on the tensor fields, $\mathcal{B}$ and $\mathcal{T}$, to those corresponding to the physical quarks. The details of this procedure are described in Ref. [23]. Performing these restrictions on the octet-baryon, quenched chiral Lagrangian [Eq. (B9)] one finds

$$\mathcal{L}^{(Q)}_{\mathcal{B}\Phi}|_R = i(\bar{\mathcal{B}}v\cdot\mathcal{D}\mathcal{B})|_R + \frac{2}{3}(2\alpha-\beta)\mathrm{tr}(\bar{B}S^\mu A_\mu B) + \frac{1}{3}(-\alpha-4\beta)\mathrm{tr}(\bar{B}S^\mu BA_\mu) + \frac{1}{3}(\alpha+4\beta+6\gamma_s)\mathrm{tr}(\bar{B}S^\mu B)\mathrm{tr}(A_\mu)$$
$$+\frac{1}{3}(2\alpha_M-\beta_M)\mathrm{tr}(\bar{B}\mathcal{M}^+B) + \frac{1}{6}(-\alpha_M-4\beta_M)\mathrm{tr}(\bar{B}B\mathcal{M}^+) + \frac{1}{6}(\alpha_M+4\beta_M+6\sigma)\mathrm{tr}(\bar{B}B)\mathrm{tr}(\mathcal{M}^+). \quad \text{(B13)}$$

Equating this with Eq. (B2) gives

$$\frac{2}{3}(2\alpha-\beta) = 2D+2F, \quad \text{(B14)}$$

$$\frac{1}{3}(-\alpha-4\beta) = 2D-2F, \quad \text{(B15)}$$

$$\frac{1}{3}(\alpha+4\beta+6\gamma_s) = 2g_s, \quad \text{(B16)}$$

$$\frac{1}{3}(2\alpha_M-\beta_M) = 2\mu b_D + 2\mu b_F, \quad \text{(B17)}$$

$$\frac{1}{6}(-\alpha_M-4\beta_M) = 2\mu b_D - 2\mu b_F, \quad \text{(B18)}$$

$$\frac{1}{6}(\alpha_M+4\beta_M+6\sigma) = 2\mu b_0. \quad \text{(B19)}$$

In extracting the flavor-singlet part, Eq. (B16) provides us with

$$\frac{1}{3}\alpha+\frac{4}{3}\beta+\sqrt{\frac{2}{3}}g_{\eta' NN}+2\gamma = \sqrt{\frac{2}{3}}g_{\eta' NN}+2\gamma_{\mathrm{QCD}}, \quad \text{(B20)}$$

and combining with Eqs. (B14), (B15) one arrives at

$$\gamma = \gamma_{\mathrm{QCD}} + D - F. \quad \text{(B21)}$$

The restrictions are much simpler for the decuplet case and one finds

$$\gamma' = \gamma'_{\mathrm{QCD}}. \quad \text{(B22)}$$

In estimating the hairpin-type couplings in full QCD one assumes that they are relatively small, $\gamma_{\mathrm{QCD}} \ll g_{\eta' NN}$, due to OZI-type suppression [43]. With analogous arguments for the decuplet, we take $\gamma_{\mathrm{QCD}} = \gamma'_{\mathrm{QCD}} = 0$. We do note that the U(1) axial anomaly may be effective in overcoming the OZI rule in the case of η' couplings [33], but as we mentioned in the text the main conclusions of our present analysis are not very sensitive to the precise value of the η'-nucleon coupling.

[1] CP-PACS Collaboration, S. Aoki *et al.*, Phys. Rev. Lett. **84**, 238 (2000).
[2] UKQCD Collaboration, K.C. Bowler *et al.*, Phys. Rev. D **62**, 054506 (2000).
[3] CP-PACS Collaboration, K. Kanaya *et al.*, Nucl. Phys. B (Proc. Suppl.) **73**, 189 (1999).
[4] C. Bernard *et al.*, Phys. Rev. D **64**, 054506 (2001).
[5] CSSM Lattice Collaboration, J.M. Zanotti *et al.*, Phys. Rev. D **65**, 074507 (2002).
[6] CP-PACS Collaboration, S. Aoki *et al.*, Phys. Rev. D **60**, 114508 (1999).
[7] G.V. Dunne, A.W. Thomas, and S.V. Wright, Phys. Lett. B **531**, 77 (2002).
[8] D.B. Leinweber, A.W. Thomas, K. Tsushima, and S.V. Wright, Phys. Rev. D **61**, 074502 (2000).
[9] J.F. Donoghue, B.R. Holstein, and B. Borasoy, Phys. Rev. D **59**, 036002 (1999).
[10] D.B. Leinweber, A.W. Thomas, K. Tsushima, and S.V. Wright, Phys. Rev. D **64**, 094502 (2001).
[11] D.B. Leinweber, A.W. Thomas, and S.V. Wright, Phys. Lett. B **482**, 109 (2000).
[12] D.B. Leinweber, D.H. Lu, and A.W. Thomas, Phys. Rev. D **60**, 034014 (1999).
[13] E.J. Hackett-Jones, D.B. Leinweber, and A.W. Thomas, Phys. Lett. B **489**, 143 (2000).
[14] D.B. Leinweber and A.W. Thomas, Phys. Rev. D **62**, 074505 (2000).
[15] T.R. Hemmert and W. Weise, hep-lat/0204005.
[16] E.J. Hackett-Jones, D.B. Leinweber, and A.W. Thomas, Phys. Lett. B **494**, 89 (2000).
[17] W. Detmold, W. Melnitchouk, J.W. Negele, D.B. Renner, and A.W. Thomas, Phys. Rev. Lett. **87**, 172001 (2001).
[18] W. Detmold, W. Melnitchouk, and A.W. Thomas, EPJdirect **13**, 1 (2001).
[19] W. Detmold, W. Melnitchouk, and A.W. Thomas, Phys. Rev. D **66**, 054501 (2002).
[20] S.R. Sharpe, Phys. Rev. D **41**, 3233 (1990).
[21] S.R. Sharpe, Phys. Rev. D **46**, 3146 (1992).
[22] C.W. Bernard and M.F.L. Golterman, Phys. Rev. D **46**, 853 (1992).
[23] J.N. Labrenz and S.R. Sharpe, Phys. Rev. D **54**, 4595 (1996).
[24] D.B. Leinweber, Nucl. Phys. B (Proc. Suppl.) **109**, 45 (2002).
[25] M.J. Savage, Nucl. Phys. **A700**, 359 (2002).
[26] R.D. Young, D.B. Leinweber, A.W. Thomas, and S.V. Wright, Nucl. Phys. B (Proc. Suppl.) **109A**, 55 (2002).
[27] A.W. Thomas and W. Weise, *The Structure of the Nucleon* (Wiley-VCH, Berlin, 2001).
[28] P.A.M. Guichon, G.A. Miller, and A.W. Thomas, Phys. Lett. **124B**, 109 (1983).

[29] A.W. Thomas and K. Holinde, Phys. Rev. Lett. **63**, 2025 (1989).
[30] J. Gasser and H. Leutwyler, Ann. Phys. (N.Y.) **158**, 142 (1984).
[31] V. Bernard, N. Kaiser, and U.-G. Meissner, Int. J. Mod. Phys. E **4**, 193 (1995).
[32] J. Gasser, M.E. Sainio, and A. Svarc, Nucl. Phys. **B307**, 779 (1988).
[33] S.D. Bass, Phys. Lett. B **463**, 286 (1999).
[34] M.N. Butler, M.J. Savage, and R.P. Springer, Nucl. Phys. **B399**, 69 (1993).
[35] Y. Kuramashi, M. Fukugita, H. Mino, M. Okawa, and A. Ukawa, Phys. Rev. Lett. **72**, 3448 (1994).
[36] W. Bardeen, A. Duncan, E. Eichten, and H. Thacker, Phys. Rev. D **62**, 114505 (2000).
[37] MILC Collaboration, T. DeGrand and U.M. Heller, Phys. Rev. D **65**, 114501 (2002).
[38] MILC Collaboration, C.W. Bernard *et al.*, Phys. Rev. D **61**, 111502(R) (2000).
[39] R. Sommer, Nucl. Phys. **B411**, 839 (1994).
[40] R.G. Edwards, U.M. Heller, and T.R. Klassen, Nucl. Phys. **B517**, 377 (1998).
[41] D.B. Leinweber, R.M. Woloshyn, and T. Draper, Phys. Rev. D **43**, 1659 (1991).
[42] D.B. Leinweber and T.D. Cohen, Phys. Rev. D **47**, 2147 (1993).
[43] F.E. Close, *An Introduction to Quarks and Partons* (Academic Press, London, 1979).